Structural Studies of Rare Earth/Transition Metal Complex Ion Systems as a Basis for Understanding Their Thermal Decomposition to Mixed Oxides

Philippa A. Brayshaw,[a] Annegret K. Hall,[a] William T. A. Harrison,[a,b] Jack M. Harrowfield,*[a,c] Dierdre Pearce,[a] Todd M. Shand,[a] Brian W. Skelton,[d] Claire R. Whitaker,[a,e] and Allan H. White[d]

Keywords: Dipicolinates / Rare earths / Crystal structures / Mixed oxides / Thermochemistry

Thermal decomposition in air of the series of complexes $[Co(NH_3)_6][Ln(dipic)_3]\cdot x H_2O$, $[Cr(en)_3][Ln(dipic)_3]\cdot y H_2O$ and $[Cr(urea)_6][Ln(dipic)_3]\cdot z H_2O$ (Ln = La – Lu, excluding Pm but plus Y; dipic = 2,6-pyridinedicarboxylate) to give oxide phases has been examined. The products were characterised by powder X-ray diffraction, magnetic and surface area measurements. From the Co-containing species, either Co_3O_4 + Ln_2O_3 or perovskite ($CoLnO_3$) products result, while the Cr-containing species provide $CrLnO_4$ phases in addition, the monazite form of $CrNdO_4$ being detected for the first time in this way. Underpinning consideration of the solid state decomposition mechanisms, single-crystal X-ray structure determinations have been performed on $[Co(NH_3)_6][Ln(dipic)_3]\cdot n H_2O$ across the Ln series, defining differing phases (all triclinic $P\bar{1}$) for n = 5 (encompassing Ln = La–Pr), n = 8(.5) (Ln = Tm – Eu) and n = 10 (Ln = Pr – Er, including Y), and also on one of the low-temperature decomposition products, $[Co(NH_3)_6]Cl\cdot dipic\cdot 2H_2O$ (**1**). The structure of **1** provides evidence that conventional π-stacking of the dipicolinate anions may be of some importance in determining the solid state array, whereas consideration of all structures involving $[Ln(dipic)_3]^{3-}$ anions indicates that "edge-to-face" interactions between dipicolinate ligands of adjacent complex anions may also be determinants of the formation of sheet-like arrays of the trianions commonly observed in these compounds.

Introduction

In the hope of gaining some understanding of the complicated events which must be involved in the thermal decomposition reactions of mixed-metal solids in which a transition metal is present in a cationic complex and a lanthanide (Ln) in an anionic complex, we have conducted a detailed crystallographic study of one family of reactants, $[Co(NH_3)_6][Ln(dipic)_3]\cdot x H_2O$, [dipic = dipicolinate = 2,6-pyridinedicarboxylate; x = 5, 8(.5), 10] and some related materials. Solids containing tris(dipicolinato)lanthanide(III) anions ($[Ln(dipic)_3]^{3-}$) have been of interest for many reasons,[1–5] but thermal decomposition reactions of their derivatives with transition metal cations to give "mixed" oxides have not been investigated. Analogous reactions, however, have been explored in numerous systems[6–11] and frequently have been found superior to those based on reactions between separate solid phases such as the monometallic oxide constituents (or their simple precursors). While mixed lanthanide/transition metal oxides have long been of interest in regard to their structural, spectroscopic, magnetic and catalytic properties, which are consequently rather well understood,[12] there remains a need to provide more efficient syntheses and better methods of control of particle size.[13] We provide herein evidence that this need may be met to some extent through the use of thermal decomposition of solids containing $[Ln(dipic)_3]^{3-}$ in association with cobalt(III) or chromium(III) complex cations. One reason for studying compounds involving a cation such as $[Co(NH_3)_6]^{3+}$ in the presence of $[Ln(dipic)_3]^{3-}$ anions was to see if the aspects of three-fold symmetry present in both species would lead to particular modes of association in their lattices which might be seen to control solid-state reactions. Interpretation of features of the supramolecular chemistry of these lattices which may be deduced from detailed analysis of their structures is enhanced by structural studies of $[Co(NH_3)_6]dipic\cdot Cl\cdot 2H_2O$ and $[Eu(dipicH)(dipic)(OH_2)_2]\cdot 4H_2O$, the latter being a member of a known

[a] Research Centre for Advanced Mineral and Materials Processing, University of Western Australia,
35 Stirling Highway, W. A. 6009, Australia
[b] Current address: Department of Chemistry University of Aberdeen,
AB24 3UE, Scotland
[c] Current address: Institut de Science et de l'Ingénierie Supramoléculaires,
8 allée Gaspard Monge, 67083 Strasbourg, France
Fax: +33-3-90245140
E-mail: harrowfield@isis.u-strasbg.fr
[d] Chemistry M313, University of Western Australia,
Nedlands, W. A. 6907, Australia
[e] Institut de Ciència de Materials de Barcelona, Campus de la Universitat Autònoma de Barcelona,
08193 Bellaterra, Cerdanyola del Valles (Barcelona), Spain
Supporting information for this article is available on the WWW under http://www.eurjic.org or from the author.

series of lanthanide complexes,[14] though both complexes were presently isolated through unintended solution decomposition reactions of two of the mixed-oxide precursor species, $[Co(NH_3)_6][La(dipic)_3]\cdot x\,H_2O$ and $[Cr(urea)_6][Eu(dipic)_3]\cdot x\,H_2O$, respectively.

Results and Discussion

1. Cobalt/Rare Earth Systems

Structure Determinations: Various hydrates, $[Co(NH_3)_6][Ln(dipic)_3]\cdot x\,H_2O$, are obtained when $[Co(NH_3)_6]^{3+}$ is precipitated from aqueous solutions by the addition of tris(dipicolinato)lanthanate(III) anions, $[Ln(dipic)_3]^{3-}$. Any given lanthanide may be a member of more than one hydrate family, thus rendering extremely complicated any attempt to fully characterise the systems. This situation is exacerbated by the fact that, although the very insoluble compounds may be readily recrystallised, the crystals obtained are often small and needle-like, thus being less than optimal for diffraction studies. To find that some adducts, slowly crystallised over periods as long as years, underwent apparent desolvation within seconds of separation from their supernatant solution was a further significant handicap. In combination, these difficulties were more acute for the heavier than the lighter rare earths. Overall, nonetheless, the gamut of the rare earth array (including Y) appears to be encompassed within three dominant series, a pentahydrate ($x = 5$) phase being defined for La – Pr, a decahydrate form for Pr – Er, Y, and an octahydrate (more precisely, an 8.5-hydrate) for Tm − Lu, these limiting members (with some intermediates) being structurally characterised herein. A broader survey, focussed particularly on hydrogen bonding in these hydrates and defining further sporadic phases, will be reported elsewhere.[15]

In all $[Co(NH_3)_6][Ln(dipic)_3]\cdot x\,H_2O$, a triclinic $P\bar{1}$ cell obtains, with one formula unit comprising the asymmetric unit of the structure. The space group $P\bar{1}$ necessarily implies a racemic mixture of the chiral anions in each case. In the penta- and "octa-"hydrate phases, the asymmetric unit of the structure is devoid of any symmetry but in the decahydrate phase, the cations lie with their cobalt atoms disposed on crystallographic inversion centres, there being two such independent species. The similarity between crystallographic *a*, *b*, *c* of the deca- and "octa"-hydrate species is noted but, seemingly, carries no deeper significance (see below). The geometries of the $[Co(NH_3)_6]^{3+}$ cations are "normal"[16] and do not justify further comment. The anions, one representative being shown in Figure 1, are also of a form already known from studies of the sodium salts,[17–20] as well as from more recent work,[1–5] with the three ligands tridentate through ONO donor atoms about the metal, making up a three-bladed propeller array of putative *32* symmetry. Their geometries are tabulated comparatively and in summary in Table 1, the most obvious trend being that expected of the "lanthanide contraction", <Ln−N> diminishing by ca. 0.22 Å across the series, and <Ln−O> by rather less, ca. 0.18 Å. The components of the geometries vary rather widely, particularly in the angles and particularly at the lighter end of the series, where it might be expected that, in the context of nine-coordination throughout, the constraints on the packing of the three ligands about the metal are less demanding. The carboxylate groups are essentially coplanar with their parent pyridine rings, albeit not rigidly so, and out-of-plane Ln deviations are substantial, even relative to the pyridine ring and most particularly among the complexes containing the lighter rare earths. There is no association of the cations and anions into intimate pairs or columns of alternating species which simply reflects common aspects of threefold symmetry.

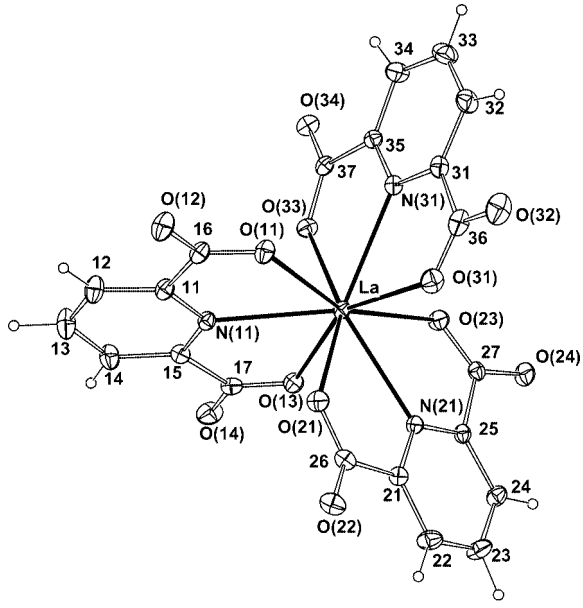

Figure 1. A view of the $[La(dipic)_3]^{3-}$ anion present within the lattice of $[Co(NH_3)_6][La(dipic)_3]\cdot 5\,H_2O$ (**2**), showing the numbering system which provides the basis for Table 1.

The component water molecules are described with variable definitiveness, those in the penta- and deca-hydrate families, respectively, being most and least precisely defined. The first structure solved was that of the pentahydrate phase of the Ce species **3**, a significant result at the time in confirming the Ce^{III} oxidation state, since the orange colour of the precursor $Na_3[Ce(dipic)_3]\cdot 15\,H_2O$ complex had led to some suspicion that it might in fact be a Ce(IV) species (as has been obtained, apparently, with a Ca^{II} counter cation[21]). A superior structural characterisation of the pentahydrate phase was ultimately obtained for the Pr (**4a**) species, where the precision of the determination is such that all hydrogen atoms in the structure have been resolved and refined in (x, y, z, U_{iso}) and are taken as indicative of the basic hydrogen bonding scheme for this family, the La species making up a third member. Powder XRD studies (see below) indicate, however, that the pentahydrate phase may well be common to the whole rare earth series, upon partial desolvation of the higher hydrates.

The decahydrate phase has been structurally characterised for Pr (**4b**), Sm (**5**), Tb (**6**), Er (**7**) and Y (**8**) and is

Table 1. Minimum, maximum and average interatomic distances [Å] and angles [°] of the lanthanoid environments for the terminal members of each phase. Atom numbering herein uses the Scheme of Figure 1 as a reference/basis.

	2	**4a**	**4b**	**8**	**7**	**9**	**10**
Ln	La-5H_2O	Pr-5H_2O	Pr-10H_2O	Y-10H_2O	Er-10H_2O	Tm-8·5H_2O	Lu-8·5H_2O
Distances							
Ln−N	2.631(2)	2.589(7)	2.580(7)	2.469(5)	2.455(4)	2.420(3)	2.404(8)
	2.656(2)	2.609(9)	2.594(9)	2.478(6)	2.469(4)	2.474(2)	2.42(1)
Average	2.64(1)	2.60(1)	2.588(6)	2.474(5)	2.463(6)	2.45(3)	2.42(2)
Ln–O	2.525(2)	2.490(2)	2.492(7)	2.391(5)	2.382(3)	2.360(3)	2.337(8)
	2.571(2)	2.537(2)	2.526(6)	2.419(4)	2.419(3)	2.408(2)	2.381(5)
Average	2.54(2)	2.50(2)	2.50(1)	2.40(1)	2.39(1)	2.38(5)	2.36(2)
Angles							
N–Ln−N	116.96(6)	117.13(6)	118.4(3)	118.1(2)	118.3(1)	117.28(8)	117.7(3)
	125.22(6)	124.65(6)	122.7(2)	122.6(2)	122.6(2)	121.80(9)	121.5(3)
Average	120(5)	120(4)	120(2)	120(2)	120(2)	120(2)	120(2)
O*n*1−Ln−O*n*+13	153.2(1)	151.26(6)	149.4(2)	145.4(1)	145.2(1)	145.58(9)	144.8(3)
	157.2(1)	154.85(5)	153.3(2)	148.4(1)	147.7(1)	147.18(7)	146.0(3)
Average	155(2)	153(2)	151(1)	147(2)	146(1)	146.5(8)	145(1)
N*n*1–Ln–O*n*1,3	60.98(7)	61.81(6)	61.9(2)	64.2(1)	64.6(1)	64.45(8)	64.7(3)
	62.05(7)	62.92(6)	62.8(2)	64.9(2)	65.1(1)	65.96(9)	66.5(3)
Average	61.4(4)	62.4(4)	62.4(3)	64.5(4)	64.9(2)	65.6(9)	65.7(8)
O*n*1–Ln–O*n*3	122.09(7)	123.87(6)	124.1(2)	129.0(2)	129.6(1)	129.01(7)	129.6(2)
	122.93(7)	125.02(5)	125.3(2)	129.3(1)	129.9(1)	131.80(8)	132.5(3)
Average	122.6(4)	124.6(6)	124.7(6)	129.2(2)	129.7(2)	130(1)	131(2)
O*nm*−Ln−O*n*±1*m*	73.36(7)	73.69(6)	73.6(2)	73.4(2)	73.3(1)	73.89(8)	74.8(3)
	80.72(8)	80.18(7)	80.4(2)	79.1(2)	78.9(1)	77.84(8)	78.0(3)
Average	77(3)	76(3)	77(3)	77(3)	76.2(12)	76.0(15)	76(5)
O*n*1−Ln−O*n*−13	87.79(8)	87.58(7)	84.0(2)	84.2(1)	84.3(1)	87.64(9)	87.3(3)
	93.18(8)	92.56(6)	93.0(2)	92.1(1)	92.1(1)	93.32(8)	93.1(2)
Average	91(3)	91(3)	90(5)	89(4)	89(4)	89(3)	90(3)
N*n*1−Ln−O*n*+11;*n*−13	73.25(7)	72.96(6)	74.3(2)	72.1(1)	72.0(1)	72.47(8)	71.9(3)
	80.55(8)	78.71(7)	79.8(2)	74.6(2)	74.3(1)	73.93(9)	73.5(2)
Average	74(3)	76(3)	76(2)	74(1)	73(1)	73.3(5)	72.7(6)
N*n*1−Ln−O*n*+13;*n*−11	131.5(1)	132.1(1)	131.7(2)	132.6(1)	132.9(1)	133.05(7)	133.4(2)
	140.0(1)	139.6(1)	139.0(2)	138.7(2)	138.8(1)	137.37(9)	135.8(3)
Average	134(3)	134(3)	135(3)	135(2)	135(2)	135(2)	135(1)
Interplanar dihedral angles							
$C_5N(1)/C_5N(2)$	86.4(1)	86.5(1)	87.7(4)	87.5(3)	87.6(2)	89.3(1)	89.4(5)
$C_5N(2)/C_5N(3)$	87.0(1)	81.8(1)	84.1(4)	82.7(3)	82.6(2)	81.7(1)	81.3(4)
$C_5N(3)/C_5N(1)$	81.7(1)	87.7(1)	83.9(4)	81.8(2)	81.6(2)	86.6(1)	87.0(5)
$C_5N(1)/CCO_2(11)$	4.8(1)	5.6(1)	1.6(3)	1.0(2)	0.6(2)	8.8(1)	2.7(5)
$C_5N(1)/CCO_2(13)$	4.6(1)	5.5(1)	3.9(4)	3.9(3)	4.2(2)	12.2(1)	9.0(5)
$C_5N(2)/CCO_2(21)$	5.5(1)	6.3(1)	8.0(4)	7.0(3)	6.6(2)	5.8(1)	6.2(5)
$C_5N(2)/CCO_2(23)$	5.6(1)	7.7(1)	7.6(4)	8.1(3)	7.8(2)	6.4(1)	6.7(5)
$C_5N(3)/CCO_2(31)$	3.0(1)	3.5(1)	4.4(4)	3.7(3)	4.1(2)	10.4(1)	10.7(4)
$C_5N(3)/CCO_2(33)$	4.4(1)	4.4(1)	1.7(4)	2.0(3)	2.5(2)	2.7(1)	2.8(5)
Ln out of plane deviations [Å]							
$C_5N(1)$	0.192(5)	0.176(4)	0.08(1)	0.05(1)	0.032(8)	0.015(6)	0.04(2)
$C_5N(2)$	0.297(4)	0.280(4)	0.01(1)	0.04(1)	0.030(8)	0.043(5)	0.06(2)
$C_5N(3)$	0.051(5)	0.042(4)	0.12(2)	0.10(1)	0.112(8)	0.228(5)	0.24(2)

presumed accessible to at least the intervening rare earths (Table 1). For this family, site occupancy refinement of water molecule oxygen sites is indicative of full occupancy of all postulated sites across the series; for all, however, the displacement parameters, possibly a foil for minor disorder, are high for a number of these, and for some no hydrogen atom locations were definitively established. Throughout the x = 8(.5) series also, solvent displacement parameters generally are high, possibly indicative of or associated with the difficulties in the crystallisation of adducts containing heavy Ln, with site occupancy refinement suggestive of some fragment populations. Unit cell projections for the various phases are shown in Figures 2(a)–(c), representative in general for each phase, although there may be variations in the fine detail of the modelling of the hydration. The complex anions, as in other structures (discussed ahead), may be considered to be disposed in homochiral columns lying side-by-side, with chirality alternating, to form sheets, viewed edge-on here, interspersed by layers of cations and associated water molecules, the two systems being interconnected by hydrogen bonds between cation, solvent and anions, in the last via the uncoordinated carboxylate oxygen atoms. In the "octa"-hydrates, the cations lie in between translation-related anions in projection down *b*, generating a CoLn column up that axis. In similar projections of the penta- and deca-hydrates, the cations lie between the anions with the axes of the Co and Ln chains parallel but not collinear. A similar motif of parallel-column/sheet formation

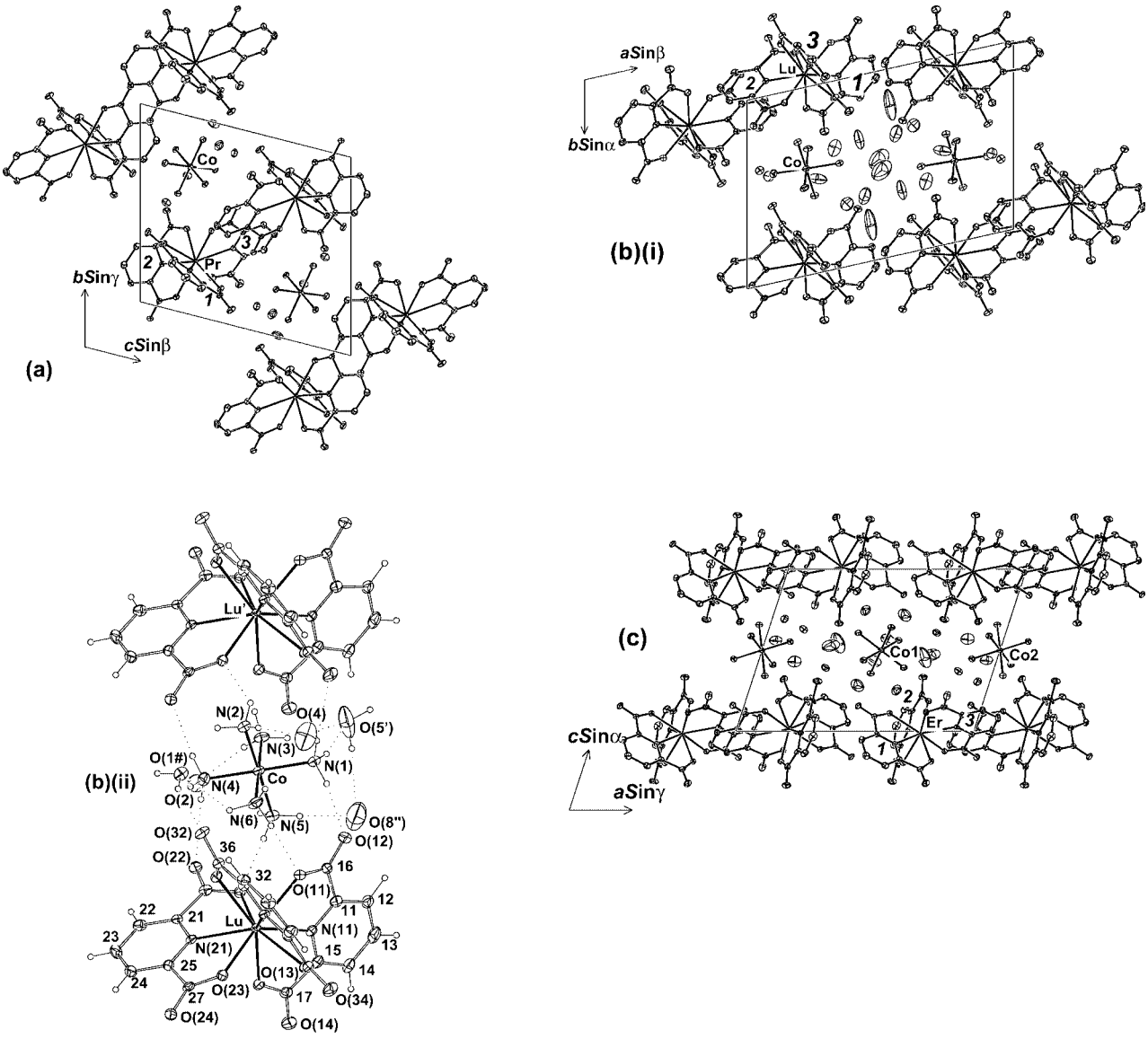

Figure 2. Representative unit cell projections for the various hydrate types $[Co(NH_3)_6][Ln(dipic)_3]\cdot x\,H_2O$, x = 5, 8(.5), 10. (a) Ln = Pr, x = 5 (**4a**), down *a*; (b) Ln = Lu, x = 8.5 (**10**), (i) down *c* and (ii) down *b*, showing the column stacking; (c) Ln = Er, x = 10 (**7**), down *b*.

is seen for the more highly charged anions of the complex $Na_5[Gd(chelidamate)_3]\cdot 16\,H_2O$[22] (chelidamic acid = 4-hydroxy-2,6-pyridinedicarboxylic acid), where approaches between anions of opposite chirality involve chelate units on the separate centres very closely parallel but with no atom separations for these rings being <3.9 Å and the closest atom approaches (3.1–3.2 Å) in fact being between uncoordinated carboxylate-*O* and C(2) of a near-orthogonal chelate ring on the adjacent centre. (Contact between anions of the same chirality appears to be mediated by H-bonding involving the 4-phenol/phenoxide groups.) In terms of the details of possible interactions, the present systems exhibit similarities but with further complications.

Thus, in the precisely defined pentahydrate-phase structure of $[Co(NH_3)_6][Pr(dipic)_3]\cdot 5\,H_2O$, the anion sheets (in planes parallel to [0,−1,1]), seen edge-on in the view down *a* [Figure 2(a)], involve each anion having two near neighbours (as part of a column) of the same chirality, with Pr···Pr 10.4500(7) Å (= *a*; homochiral contact), and three near-neighbours of opposite chirality, with Pr···Pr 8.4476(4), 8.6449(4) and 9.3568(4) Å (heterochiral contacts). The homochiral pairs are rather remote, with the only close approaches involving atoms in near orthogonal chelate units, so that they are perhaps best described as of a "edge-to-face" type,[23] (or possibly as a bent CH···O interaction) involving O(uncoordinated)···C(2) 3.458(4) Å and O(coordinated)···C(3) 3.576(4) Å. For the heterochiral pairs, interpenetration of the coordination spheres involves pairs of chelates being closely parallel but this is duplicitous evidence for stacking in that either ring atoms are not overlapped in projection or the ring planes are separated by >3.6 Å. Thus, both the 8.4476 and 8.6449 Å pairs involve

parallel rings for which only the C–O(uncoordinated) units overlap in projection, involving C···O separations of 3.020(3) and 2.911(3) Å, respectively. For the 9.3568 Å pair, while the parallel ring overlap in projection is more extensive, all interatomic separations are >3.6 Å and possible edge-to-face interactions involving coordinated-*O* to C(4) and C(3) of a nonparallel ring lead to significantly shorter contacts [3.566(3) and 3.585(3) Å, respectively]. In an "octa"hydrate species such as $[Co(NH_3)_6][Lu(dipic)_3]\cdot 8.5H_2O$, where the anion sheets are seen edge-on in the view down *c* [Figure 2(b)], both homochiral [10.419(5) Å] and heterochiral [8.571(4), 8.860(5) and 9.328(4) Å] unit separations involve quite similar juxtapositioning of the anions to those in the Pr pentahydrate compound, though involving differences in specific interatomic approaches consistent with a very complicated balance of forces being involved. The closest contact in the homochiral pair, 3.291(2) Å, is that of a dipicolinate C(3) to an uncoordinated-*O* of a near-orthogonal chelate unit, again possibly an edge-to-face aromatic or a bent CH···O interaction. The adjacent C(4) is 3.46(1) and 3.58(2) Å, respectively, from uncoordinated- and coordinated-*O* of the same carboxylate and these are the only contacts which could be termed close. For the heterochiral pair at 8.571 Å, stacking C···O contacts are apparent at 3.24(1) Å but the 8.860 Å pair is less like its Pr analogue in that the closest (stacking) contacts are C(aromatic)···C(carboxylate) at 3.406(2) Å and two C(aromatic)···C(aromatic) at 3.461(2) Å. The closest contact in the heterochiral 9.328 Å pair is a C(4)···O(coordinated) separation of 3.461(2) Å, again involving atoms in nonparallel rings. In a decahydrate such as $[Co(NH_3)_6][Er(dipic)_3]\cdot 10H_2O$, where the anion sheets are seen edge-on in the view down *b* [Figure 2(c)], there are no contacts <3.7 Å between atoms in the homochiral pairs [11.227(1) Å = *b* apart] and while in the closest heterochiral pair [8.468(9) Å apart], there are stacking contacts C(carboxylate)···O(uncoordinated) of 3.422(8) Å, the closest atomic separation is 3.310(7) Å for O(uncoordinated)···O(coordinated). For the more remote pair 8.588(7) Å apart, the parallel ring positions are very similar but just sufficiently different to those of the 8.468 Å pair for C(carboxylate)···O(uncoordinated) at 3.226(8) Å to now be shorter than C(carboxylate)···O(uncoordinated) (3.313(8) Å] and O(uncoordinated)···O(coordinated) [3.346(8) Å]. For the longest heterochiral pair separation [9.269(9) Å], despite two rings being closely parallel and having significant overlap in projection, no interatomic separations are <3.6 Å, though several are close to this value. All these subtleties in the detail of what can be grossly termed "aromatic-aromatic" interactions can also be discerned in many structures of simpler materials such as metal nitrophenoxides and other aza-aromatic carboxylates,[24,25] as well as in structures of complexes of neutral aza-aromatic ligands.[23] How significant particular separations may be and how they may be related to lattice energies are nontrivial issues but the individual interaction energies are presumably small[23] and it may be noted that, across the various $[Co(NH_3)_6][Ln(dipic)_3]\cdot xH_2O$ phases, the cell dimensions are not too dissimilar, suggestive of a relatively facile passage from one form to another, possibly with rather minimal energy differences, in the course of crystallisation.

While the segregation of $[Ln(dipic)_3]^{3-}$ anions into sheet-like structures in all the cases described above might be taken as indicative of energetically important interactions, particularly those involving heterochiral pairs, between the anions, it is instructive to apply a similar analysis to the structures of other known derivatives. First structurally characterised were the sodium compounds and in $Na_3[Nd(dipic)_3]\cdot 15H_2O$,[18] for example, while again anion sheets generated from a side-by-side, alternating arrangement of homochiral columns can be discerned, one heterochiral pair involves closely parallel rings but with no ring atom separations <4 Å and another closely parallel rings with no separation <3.5 Å, suggesting any stacking to be of minimal importance. For the closest homochiral pair [10.353(15) Å = *a* apart], the only close contacts are C(3)···O(uncoordinated) and C(4)···C(carboxylate) of 3.25 and 3.30 Å, respectively. In the monoclinic form of $Na_3[Yb(dipic)_3]\cdot 13H_2O$,[17] racemic anion sheets are present but can no longer be regarded as built up from side-by-side positioning of homochiral columns containing anions in a common orientation. Concomitantly, heterochiral pairs involve closely parallel ring arrangements but none of this apparent stacking involves atomic approaches <3.6 Å and only for one pair is there a close edge-to-face contact [C(3)···O(uncoordinated)] of 3.37 Å. The closest homochiral pair involves a relative orientation unlike that in the Nd compound which results in one C(4)···C(4′) contact of 3.46 Å. In orthorhombic $Na_3[Yb(dipic)_3]\cdot 14H_2O$,[17] an anion sheet built up of adjacent homochiral columns is recovered but no pair within it involves short interatomic contacts aside from C(4)···C(carboxylate) and C(4)···O(uncoordinated), both close to 3.5 Å in the heterochiral pair 9.76 Å apart. In the similar anion sheet of $Na_4[Yb(dipic)_3][ClO_4]\cdot 10H_2O$,[19] close contacts are again rare, only edge-to-face C(3,5)···O(uncoordinated) at 3.31 Å in the homochiral pair 10.37 Å apart being obvious. Such results may mean that the anion sheet is a flexible motif, adjusting to restraints imposed by other components of the lattice. Consistent with this is the presence of homochiral sheets in $Cs_3[Eu(dipic)_3]\cdot 9H_2O$[1a] [with closest interatomic contacts being C(3,5)···O(uncoordinated) 3.44(2) Å] and the presence of racemic sheets in $[Co(sar)][Eu(dipic)_3]\cdot 13H_2O$[1a] (sar = "sarcophagine" = 3,6,10,13,16,19-hexaazabicyclo[6.6.6]icosane) where there is no evidence of any significant stacking. $[N(CH_2CH_3)_4]_3[Eu(dipic)_3]\cdot 4H_2O$[1c] provides a complicated system in which sheets of anions can be discerned which alternate in the sense that the orientations of the anion, common within a sheet, are nearly orthogonal from one sheet to the next. In one sheet, only homochiral pairs involve any close interatomic approaches, very similar to those in $Na_4[Yb(dipic)_3][ClO_4]\cdot 10H_2O$, with C(3,5)···O(uncoordinated) 3.33 Å. In the other sheet, homochiral pair contacts are similar, with a separation of 3.39 Å but the heterochiral pairs 10.29 Å apart appear to involve stacking, with C(3)···C(3′) 3.42 and C(4)···C(4′) 3.43 Å. The tet-

raethylammonium cation is, of course, unlike all other countercations discussed so far in that it is formally neither an H-bond donor nor a coordinating centre, properties shared with cations such as $[Co(bipy)_3]^{3+}$ and $[Co(phen)_3]^{3+}$. These cations also give $[Ln(dipic)_3]^{3-}$ derivatives with rather different anion arrays, their properties being described in detail elsewhere.[26] $[NEt_4]^+$ is not like these cations in having an aliphatic exterior and there are approaches indicating possible CH···O interactions with dipicolinate carboxylate-*O*, as in fact there are for the butyl chain in the complex $[Co(3\text{-butyldiamsar})][Sm(dipic)_3]\cdot 15H_2O$ ("diamsar" = 1,8-diaminosarcophagine).[27]

Of the various forces in addition to anion−anion (aromatic) interactions which may determine the lattice arrays, important in the present systems would appear to be familiar H-bonding (discussed in more detail elsewhere[15]) and metal ion coordination. In addition to the columnar arrays of anions referred to above, it is possible to discern in many instances columns in which anions are bridged by cations and/or water. In all $[Co(NH_3)_6][Ln(dipic)_3]\cdot x H_2O$, as well as $Na_3[Nd(dipic)_3]\cdot 15H_2O$,[17] $Na_3[Yb(dipic)_3]\cdot NaClO_4\cdot 10H_2O$[19] and $Cs_3[Eu(dipic)_3]\cdot 9H_2O$,[1a] the metal ions align in such a way that the lanthanide and the other cation alternate in a chain, with the C_3 axes of the $[Ln(dipic)_3]^{3-}$ anions being oriented along the chain and with the structural indications being that coordination (of an alkali metal) or H-bonding (of Co–NH_3) to the "*exo*" dipicolinate oxygens atoms determines or assists this feature of the total crystalline array. In orthorhombic $Na_3[Yb(dipic)_3]\cdot 14H_2O$,[17] however, no such "mixed" chains are found and the C_3 axes of the anions appear to lie in the *bc* plane with alternating tilts towards Na^+ columns parallel to *c*. This may be associated with size differences between Nd^{3+} and Yb^{3+} in this hydrate series, where it is apparent also that the $[Yb(dipic)_3]^{3-}$ species is significantly distorted from true D_3 symmetry and the Yb columns can be regarded as forming pairs parallel to *b*. The Yb environment appears more symmetrical in monoclinic $Na_3[Yb(dipic)_3]\cdot 14H_2O$[19] and the C_3 axes of the complex anions seem more closely aligned (here, parallel to *a*) but again sodium cations are not directly interposed between Yb ions in columns. Although it is possible for $[Co(NH_3)_6]^{3+}$ to orient three NH bonds on a trigonal face parallel to the threefold axis of the octahedron, it does not adopt this mode to interact with the threefold symmetric dipicolinate *exo*-O_3 array of a given anion, presumably because of dimensional mismatching, but it is nonetheless apparent from the structure of $[Co(sar)][Eu(dipic)_3]\cdot 13H_2O$[1a] that in this case the fixed orientations of the NH bonds of the cation away from its C_3 axis are the likely cause of the juxtaposition (down *b*) of columns of the cations adjacent to columns of the anions (with their C_3 axes oriented down *b*). A similar feature is apparent in the structure of the $[Cr((NH_2)_2sar)][Ln(dipic)_3]\cdot 8H_2O$ series,[1b] even though here some differences might be expected because of the presence of the terminal primary amino groups. In both cases, anyway, the interactions between a given cation-anion pair are only part of an extended structure involving lattice water as well. Any asymmetry in the overall formal charge distributions on the cation and anion must of course be considered as another influence on cation-anion orientation and the rather beautiful sinusoidally undulating cation and anion sheets observed in $[Cr((NH_3)NH_2sar)][Cr((NH_3)_2sar)][La(dipic)_3]_3\cdot 32H_2O$[1b] provide evidence of its possible effects.

A specific aspect of interest in the solid-state structures of mixed transition metal/rare earth compounds is the influence of particular features of the structure on the separation and consequent degree of interaction between the different metal centres. The least separation of the Co and Ln centres within the asymmetric units of the present series varies from 5.752(3) Å in the 8.5 hydrate of the Lu species to 6.169(4) Å in the pentahydrate of the La species, all such Co···Ln separations being significantly shorter than the Cr···Ce separation in $[Cr\{(NH_2)_2sar\}][Ce(dipic)_3]\cdot 8H_2O$ (7.054(2) Å)[1b] and the Co–Eu separation in $[Co(sar)][Eu(dipic)_3]\cdot 13H_2O$ [6.733(3) Å – note an incorrect minimum of 7.408(3) Å was quoted in ref.[1a]], though still much longer than the Cs–Eu separation in $Cs_3[Eu(dipic)_3]\cdot 9H_2O$ [4.584(2) Å][1a] (where the Cs is directly coordinated to dipicolinate oxygen atoms). The relatively short Co···Ln approaches in the present compounds (and note that, for all, there is another only slightly longer) presumably reflects the fact that some of the coordinated ammonia ligands appear to be involved in direct hydrogen bonding to dipicolinate oxygen atoms though, as indicated by the Co···Pr separations in the pentahydrate and decahydrate species, 6.1629(6) and 5.9143(9) Å, respectively, water also acts as a "glue" which is more effective the greater its abundance. It is also notable that in the series of hydrated sodium salts, $Na_3[Ln(dipic)_3]\cdot x H_2O$,[17–20] the shorter Ln..Ln separations occur in the lattices of the earlier and larger Ln^{3+} ions, again in association with a (here, slightly) higher degree of hydration. The subtleties of these issues are further illustrated by the facts that: (i) in the $[Cr\{(NH_2)_2sar\}][Ln(dipic)_3]\cdot 8H_2O$ series,[1b] Cr···Lu [7.097(5) Å] is longer than its counterpart Cr···La [7.051(7) Å], while Cr···La (x, $y-1$, z), at 7.097(9) Å contracts to a counterpart Cr···Lu value of 6.991(6) Å; (ii) that in the present $[Co(NH_3)_6][Ln(dipic)_3]\cdot 10H_2O$ family, the minimum Co···Ln [5.9143(5) (Pr), 5.880(1) (Sm), 5.8747(9) (Tb), 5.8719(4) Å (Er)] decreases in agreement with the lanthanide contraction but by an amount which is les than half the change in Ln-donor atom bond lengths. The lanthanide-transition metal ion separations observed in the present system must be close to the minima possible if both metals are to retain independent coordination environments but they considerably exceed the separations found between lanthanide ions in binuclear calixarene complexes where significant but very weak metal-metal interactions can be detected.[28]

Crystals of $[Co(NH_3)_6]dipic\cdot Cl\cdot 2H_2O$ (**1**) were first isolated as a result of decomposition reactions occurring during first attempts to recrystallise $[Co(NH_3)_6][La(dipic)_3]$, though it was discovered after the structural study had been completed that orange, needle-like crystals of the same material slowly deposited on simply mixing solutions of $[Co(NH_3)_6]Cl_3$ and disodium dipicolinate. A representation

of the structure, viewed down *a*, is given in Figure 3(a). An unusual feature is that three formula units constitute the asymmetric unit. Viewed parallel to the *a* axis, the three inequivalent units appear to be related by pseudo-2_1-screw operations parallel to *c* but this is only approximately true for one of the units, and both the number of "observed" reflections and systematic absences are inconsistent with a smaller cell. Throughout the cell, in a sheet about $y = 0.5$,

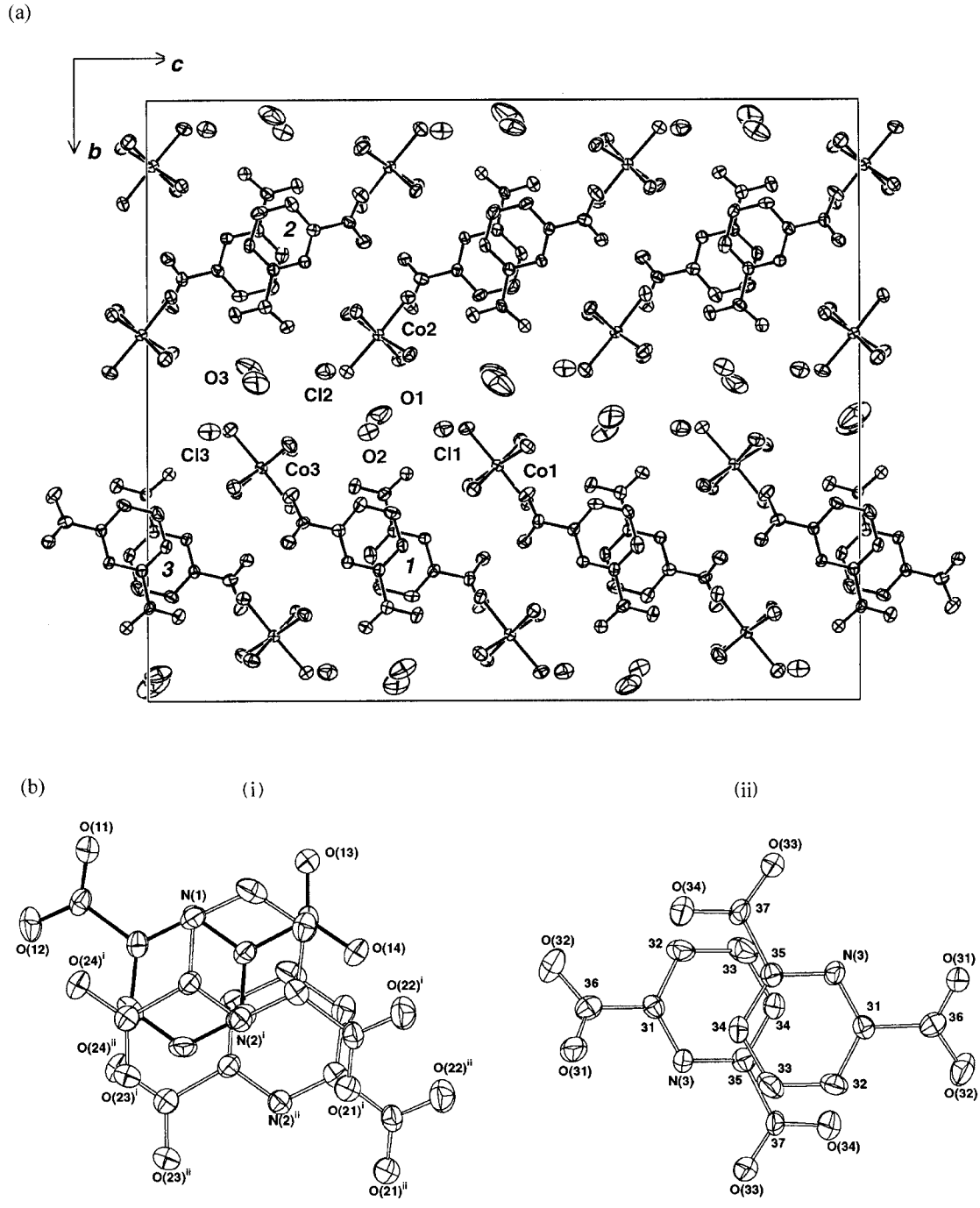

Figure 3. (a) Unit cell contents of $[Co(NH_3)_6]$dipic·Cl·$2H_2O$ (**1**), projected down *a*. (b) Interanion overlaps between; (i) anions 1 and 2, perpendicular to the aromatic plane of anion 1 (i: $1 - x$, $^1/_2 + y$, $^1/_2 - z$; ii: $2 - x$, $^1/_2 + y$, $^1/_2 - z$). N(1) contacts C(Ar) of ligand 2^i at 3.360(9), N(2^i) C(Ar) of ligand 1 at 3.387(9), the latter also contacting C(Ar) of ligand 2^{ii} at 3.54(1) Å.; (ii) anion 3 and its image ($x - ^1/_2$, $^3/_2 + y$, $\bar{z}$); C(34)···C(35) is 3.496(9) Å.

there is a complicated hydrogen-bonding network involving the water molecules, chloride and carboxylate anions and the ammonia groups of the cations. This is a common situation in "crystallised ion pairs" of polycarboxylate anions and amine complexes[29] and the very complicated nature of the system contrasts with the rather elegant simplicity of other systems incorporating polyamidinium cations and polycarboxylates.[30] by (presumed) hydrogen-bonding interactions, the "inner" oxygen atoms of a dipicolinate anion *quasi*-chelate one hexamminecobalt(III) cation while the outer oxygen atoms bridge to other hexammine cations. In the view presented in Figure 3(a), it is apparent that the dipicolinate entities lie in columns, with one molecule projecting upon the next in its column in a manner suggestive of π-stacking interactions, consistent with the fact that when viewed down *b*, the dipicolinates form undulating sheets *a*/2 = 3.56 Å apart. This is to ignore some subtleties of the array, however, in that there are dipicolinate columns down *a* of three types, two with the dipicolinate ring planes close to parallel but with their ring plane vectors oppositely oriented relative to *a* and one where the ring plane orientations alternate down the column between those of the other columns. These are associated with three types of adjacent ring projections and thus different short interatomic approaches, as shown in Figure 3(b). The anion array is quite reminiscent of that known for the sodium complex, [Na(dipicH)(dipicH$_2$)(OH$_2$)$_3$],[31] where layers are separated by *a*/2 = 3.44 Å. Dipicolinate stacking is also apparent in the lattice of [Eu(dipicH)(dipic)(OH$_2$)$_2$] and its congeners.[14]

Powder Diffraction Studies of Hydration

The powder diffraction pattern predicted[32–34] from the single crystal structure determined for [Co(NH$_3$)$_6$][Ce(dipic)$_3$]·5H$_2$O (**3a**) was in good agreement with that observed for the bulk sample rapidly crystallised from water and stored under ambient (low humidity) conditions, indicating that the pentahydrate phase may be readily isolated. On the first occasion that several members of the complete [Co(NH$_3$)$_6$][Ln(dipic)$_3$]·*x*H$_2$O series were isolated under essentially identical conditions, the La (**2**), Ce (**3**) and Pr (**4a**) compounds all gave this powder pattern. However, a clearly different powder pattern was observed for the Sm (**5**) and Eu derivatives and yet another for the Dy, Ho and Yb derivatives. The 2θ angles of the most intense peak in these powder spectra were found to be 8.70–8.80° for La, Ce, Pr, 8.25–8.30° for Sm and Eu, and 9.35–9.40° for Dy, Ho and Yb but after the Sm and Ho compounds, for example, had been heated at 50 °C under vacuum for several hours, both provided a powder pattern with the most intense peak having 2θ = 8.75°. Extended, later studies of the complete series showed that if the samples were thoroughly ground prior to the recording of powder diffraction spectra (so, presumably, allowing rapid equilibration of crystal hydrate water with atmospheric humidity), the powder patterns for all compounds were close to that predicted for the pentahydrate phase. The facts that subsequent crystal structure determinations (described above and to be reported elsewhere) showed that other (higher) hydrates could be isolated at least as larger crystals and that the predicted powder pattern for the Lu species[33] closely corresponded to that first observed for the Dy, Ho and Yb compounds we interpret, in conjunction with the first observations, as indicating that the [Co(NH$_3$)$_6$][Ln(dipic)$_3$] compounds may precipitate as various hydrate mixtures but that the pentahydrate phase is preferred for the solid materials stored under ambient conditions.

Thermogravimetry

Qualitatively, thermograms over the range of ca. 25–800 °C obtained for all the [Co(NH$_3$)$_6$][Ln(dipic)$_3$]·*x*H$_2$O compounds were identical, showing the features expected from the behaviour of related, simpler compounds. Data for the Ln = La and Lu compounds are shown in Figure 4(a). The major mass change between 400–470 °C is associated with evolution of heat and corresponds with the major exotherm observed for [Co(NH$_3$)$_6$]dipic·Cl·2H$_2$O (**1**), so that

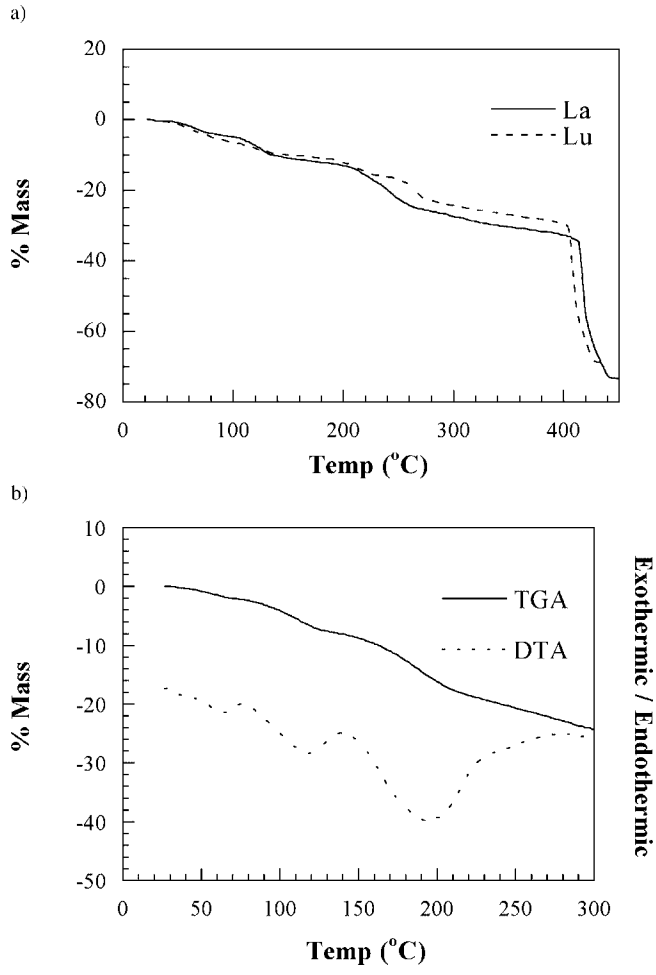

Figure 4. (a) Mass changes during thermal decomposition of [Co(NH$_3$)$_6$][Ln(dipic)$_3$]·*x*H$_2$O (Ln = La, Lu) in air. (b) Initial mass changes during thermal decomposition of [Co(NH$_3$)$_6$][Ce(dipic)$_3$] ≈ 6H$_2$O in air.

we assume it to reflect the oxidative decomposition of dipicolinate.[10] The significantly endothermic events occurring between ca.200 and 300 °C are similar to those of both **1** and $[Co(NH_3)_6]Cl_3$ in this range (note that the latter complex displays no strong exotherm at higher temperatures) and are thus associated with at least the final steps in the decomposition of the $[Co(NH_3)_6]^{3+}$ moiety. The mass changes below ca. 200 °C, all of them associated with weak endotherms, were of particular interest given the crystallographic characterisation of different hydrates across the rare earth series but from observation of the mass changes alone and without monitoring of the evolved gases, it is not possible to clearly distinguish water and ammonia loss processes in this range. However, the most readily induced changes (below 100 °C) can be reversed by exposure of the solids to humid air, so that it is assumed that these are simply associated with reversible dehydration. A thermogram for the Ln = Ce compound between ambient temperature and 250 °C is shown in Figure 4(b). The starting material for this experiment was previously equilibrated in air of 75% relative humidity (298 K)[36] to ensure a reproducible composition, though microanalyses (C, H, N) indicated a formulation intermediate between that of a hexahydrate and a pentahydrate and presumably the bulk sample may have contained several phases. Repetitive thermograms provided the mean results of a near mass plateau at 75 ± 10 °C corresponding to a weight loss of 4.8 ± 0.9% (i.e., ≈ $2H_2O$) and another at 113 ± 5 °C corresponding to a total weight loss of 12.2 ± 1.4% (i.e., ≈ $6H_2O$ overall, though a contribution from ammonia loss cannot be excluded). The stepwise loss of water is consistent with the fact that the crystal structure determination on the pentahydrate shows that the lattice water molecules are in inequivalent sites, so that some differences in their rates of thermal release would be expected.

After being heated to 600 °C or higher in air, all the $[Co(NH_3)_6][Ln(dipic)_3]\cdot x H_2O$ solids were converted to black powders for which microanalysis showed negligible carbon and nitrogen contents. Powder diffractometry (see below) confirmed that these powders were metal oxides. Scanning electron micrographs of the products obtained after ca. 15 min at 600 °C from the Pr and Lu compounds showed the different products to have different particle morphologies but with a similar mean particle size ca.2 μm.

Powder Diffractometry of Thermal Decomposition Products

Phase equilibria in Co/Ln/O systems have been thoroughly studied,[12] so that it was anticipated that perovskite, $CoLnO_3$, materials might be observed as the products of the thermal decomposition reactions. Powder diffractometry showed this expectation to be justified, though, again as expected, generation of the perovskite phase from the separate monometallic oxides appeared to become more difficult in progressing from the lighter to the heavier rare earths. Thus, under the conditions of our experiments, only Co_3O_4 and Ln_2O_3 could be detected as products for Ln = Yb, Lu. In fact, Co_3O_4 and Ln_2O_3 were the initial products in all cases, indicating that there could be no particular advantage to synthesis of the perovskites by thermal decomposition of $[Co(NH_3)_6][Ln(dipic)_3]\cdot x H_2O$ rather than by direct reaction of the oxides. This initial formation of separate oxide phases may be consistent with the observed decomposition during attempted recrystallisation in that dipicolinate release could result from the (solid state) hydrolysis reaction

$$[Ln(dipic)_3]^{3-} + 3H_2O \rightarrow [Ln(OH)_3] + 3Hdipic^-$$

giving a separate rare earth phase prior to any decomposition of the $[Co(NH_3)_6]^{3+}$ unit. The self-association of "free" dipicolinate units through π-stacking may be a factor favouring the early occurrence of this reaction. The kinetic inertness and high stability of the $[Co(NH_3)_6]^{3+}$ cation is probably another reason why a dipicolinate-bridged Co/Ln species which might smoothly transform to a mixed oxide is not formed.

2. Chromium/Rare Earth Systems

The $[Cr(en)_3][Ln(dipic)_3]\cdot x H_2O$ solids are all light-sensitive and the initially clear-yellow crystals precipitated from aqueous solution turn violet within several hours on exposure to normal ambient levels of illumination. For this reason, we have made a study of only a few members of the series to ensure that there are no dramatic differences in thermal behaviour from that of their $[Cr(urea)_6][Ln(dipic)_3]\cdot x H_2O$ analogues (which, as expected, are much less light-sensitive). The green $[Cr(urea)_6][Ln(dipic)_3]\cdot x H_2O$ compounds are particularly insoluble, precipitating very rapidly as powders, and we have been unable yet to grow crystals suitable for single-crystal structure determinations. However, their powder diffractograms show a common pattern of lines for the whole series, indicating a common hydrate stoichiometry (x = 7 on the basis of microanalysis).

Thermogravimetry

Weight losses and heat exchanges occurring on heating samples of both $[Cr(en)_3][Ln(dipic)_3]$ and $[Cr(urea)_6][Ln(dipic)_3]$ compounds are unremarkable and, as with the $[Co(NH_3)_6][Ln(dipic)_3]$ compounds, the most prominent feature of the thermograms is the major mass loss and exotherm initiated near 450 °C, again assumed to be associated with decomposition of the dipicolinate units. The chemical properties of the oxide products obtained at this point appeared to be independent of the particular precursor used (at least in the cases of Ln = La, Pr, Eu, Yb and Y) but the changes occurring on further heating at higher temperatures were considerably more complicated than in the Co systems. They were studied in detail for the products from the $[Cr(urea)_6][Ln(dipic)_3]$ precursors using powder diffractometry of the solids after periods of oven-heating at various temperatures between 450 and 900 °C.

Powder Diffractometry of Thermal Decomposition Products

Phase equilibria are again well-characterised for Cr/Ln/O systems,[12] so that the formation of both "chromate", $LnCrO_4$, and "chromite" (perovskite), $LnCrO_3$, solids was expected. Excepting only $[Cr(urea)_6][Ce(dipic)_3]$, which gave rise to a stable mixture of CeO_2 and Cr_2O_3, this was the case for all the compounds studied. A significant difference from the Co systems, however, was that the separate monometallic oxide phases could not be detected as intermediate products prior to the formation of the chromate or chromite phases. This may reflect a greater lability of the Cr^{III} cations compared to $[Co(NH_3)_6]^{3+}$, so that a dipicolinate-oxygen-bridged species, say, may be produced early on in the decomposition, although another significant observation is that the chromates, formally containing a Cr^{V} species, appear to be produced prior to the chromites, formally containing Cr^{III} (as in the reactant). It is difficult to establish the exact sequence of events near the actual point of oxide formation, since the product formed between 450 and 500 °C (following the major dipicolinate exotherm) is black or very dark green in colour and apparently amorphous, giving very broad lines in its X-ray diffraction pattern and an increase in temperature and/or prolonged heating are required to form materials giving identifiable powder diffraction lines. In general, nonetheless, the amorphous black initial product undergoes a conversion to a dark green, crystalline chromate phase (which is dimorphic) and then to an olive-green, crystalline chromite phase. Table 2 contains a summary of observations across the full series of compounds. Included are our measurements made to date of surface areas of the oxides, showing that high surface area materials can be readily produced through these decomposition reactions. Also interesting in relation to catalytic activity of the mixed oxides is the fact that in early experiments conducted in crucibles with (loose fitting) lids, the chromate species were observed to persist to higher temperatures. Assuming the lid to cause retention of CO_2 generated during the dipicolinate decomposition, this may indicate that the oxides effectively catalyse the CO_2/CO interconversion.

In the particular case of the thermal decomposition of $[Cr(urea)_6][Nd(dipic)_3]$, careful observation of the powder patterns of the products produced between 450 °C and 550 °C provided evidence for the hitherto unknown monazite phase of neodymium chromate being produced along with the known zircon phase. Rietveld refinement confirmed the presence of both monoclinic monazite-type [a = 6.9226(7), b = 7.1148(7), c = 6.6088(6) Å, β = 105.318(6)°, V = 313.94(7) Å^3] and tetragonal zircon-type [a = 7.3101(3), c = 6.3982(3) Å, V = 341.91(4) Å^3] in a sample prepared

Table 2. Reaction conditions and product characteristics for thermal decomposition of $[Cr(urea)_6][Ln(dipic)_3]\cdot 7H_2O$ in air.

Ln	Time / temperature	Product	Phase[a]	BET surface area [m^2 g^{-1}]
La	1 h / 550 °C	$LaCrO_4$	M	12.2
La	1 h / 600 °C	$LaCrO_4$	M	14.2
La	1 h / 700 °C	$LaCrO_3$	P	5.0
Ce	all conditions	$CeO_2 + Cr_2O_3$	–	–
Pr	1 h / 500 °C + 1 h / 550 °C	$PrCrO_4$	M / Z	11.5
Pr	1 h / 550 °C	$PrCrO_4$	M (traces Z)	15.0
Pr	1 h / 700 °C	$PrCrO_3$	P	8.1
Nd	1 h / 550 °C + 1 h / 580 °C	$NdCrO_4$	Z	8.7
Nd	1 h / 530 °C	$NdCrO_4$	M / Z	13.4
Nd	1 h / 700 °C	$NdCrO_3$	P	7.1
Sm	1 h / 600 °C	$SmCrO_4$	Z	12.7
Sm	1 h / 700 °C	$SmCrO_3$	P	19.3
Eu	1 h / 600 °C	$EuCrO_4$	Z	9.7
Eu	1 h / 700 °C	$EuCrO_3$	P	10.1
Gd	1 h / 600 °C	$GdCrO_4$	Z	7.7
Gd	1 h / 700 °C	$GdCrO_3$	P	10.2
Tb	1 h / 550 °C + 1 h / 580 °C	$TbCrO_4$	Z	13.5
Tb	1 h / 700 °C	$TbCrO_3$	P	5.5
Dy	1 h / 580 °C + 1 h / 600 °C	$DyCrO_4$	Z	18.0
Dy	1 h / 700 °C	$DyCrO_3$	P	15.2
Ho	4 h / 600 °C	$HoCrO_4$	Z	7.6
Ho	1 h / 700 °C	$HoCrO_3$	P	12.7
Er	6 h / 600 °C	$ErCrO_4$	Z	6.5
Er	24 h / 620 °C	$ErCrO_3$	P	16.5
Er	3 h / 700 °C	$ErCrO_3$	P	7.4
Tm	9 h / 600 °C	$TmCrO_4$	Z	7.9
Tm	3 h / 700 °C	$TmCrO_3$	P	14.7
Yb	5 h / 700 °C	$YbCrO_3$ (traces of Yb_2O_3)	P	13.1
Lu	3 h / 700 °C	$LuCrO_3$ (traces of Lu_2O_3)	P	11.4
Y	4 h / 600 °C	$YCrO_4$	Z	28.6
Y[b]	4 h / 600 °C	$YCrO_4$	Z	15.0
Y	5 h / 700 °C	$YCrO_3$	P	4.5

[a] M = monazite type, Z = zircon type, P = perovskite. [b] $[Cr(en)_3][Ln(dipic)_3]$ reactant.

under optimum conditions of one hour's heating at 530 °C. These well-known ABO_4-type structures, which consist of alternating [001] stacks of AO_9 polyhedra and BO_4 tetrahedra (monazite) or AO_8 and BO_4 groups (zircon) have been described in detail elsewhere.[37,38] In both structures, which are nominally related by tetrahedral rotations about [001], the O atoms are three coordinate to two rare earth cations and one tetrahedral cation. This is the first report of the monazite form of $NdCrO_4$, though the precision of the atomic positional parameters and derived geometrical data is only mediocre and neutron diffraction data would be required for a high-precision structure determination of monoclinic $NdCrO_4$. The tetragonal $NdCrO_4$ cell parameters are in good accordance with those determined earlier (a = 7.315, c = 6.399 Å) from X-ray powder data.[39] Comparison of phase fraction scale factors indicated that the ratios of the two phases in the mixture analysed was approximately 1:1. So far, we have not been able to prepare the monazite form in greater purity.

Thus, the monazite structure is now confirmed for $LnCrO_4$ (Ln = La, Pr and Nd) and the zircon structure for Ln = Pr to Yb (excluding Pm and Tm). A plot[40] of ^3V (V = unit cell volume) vs. ionic radius of the rare earth cations (Figure 5) shows smooth, approximately linear relationships for each of the two structure types. The overall trend for the $LnCrO_4$ phases is comparable to the situation for the $LnPO_4$ family,[37] where the break point between the large lanthanide (monazite) and small lanthanide (xenotime/zircon) structures occurs between Gd and Tb. Unlike the phosphates, two of the chromates, $PrCrO_4$ and $NdCrO_4$, show polymorphism between these two forms. The monazite-type polymorphs of $PrCrO_4$ and $NdCrO_4$ have smaller unit cell volumes (by ≈ 8.4 and 9.0%, respectively) than their zircon modifications, even though the rare earth cations have a higher coordination number in the monazite phases. This phenomenon has also been observed for the monazite and zircon polymorphs of thorium silicate, $ThSiO_4$, and correlated with void space and short O..O contacts in the zircon-type phase.[41] Another phase which shows polymorphism between monazite and zircon forms is $CeVO_4$.[38] The stable room-temperature polymorph of this material is monazite, with the zircon form stable above ≈ 1300 °C at ambient pressure. Under more extreme conditions ($T >$ ≈ 500 °C, $P >$ ≈ 27 kbar), $CeVO_4$ transforms again to the scheelite ($CaWO_4$) structure.

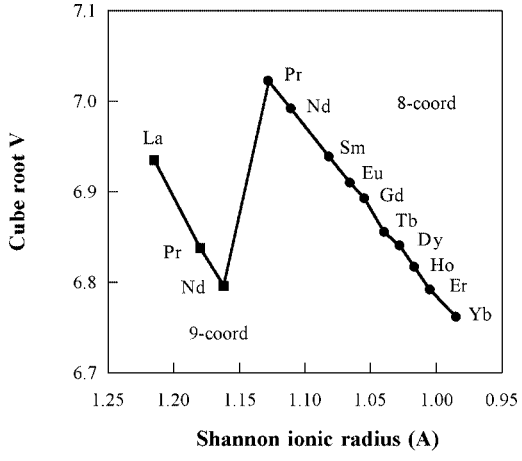

Figure 5. The relationship between unit cell volume and estimated cation radius for the monazite and zircon families of rare earth chromates.

Oxide Phase Magnetic Properties

Measurements (deposited as Supporting information; for supporting information see also the footnote on the first page of this article) of magnetic susceptibility on a selection for both the Co and Cr containing mixed oxides provided no evidence of significant differences from known data[42] for the same oxides prepared by conventional methods, and hence were not pursued in detail.

Conclusions

The work described herein provides evidence that the dipicolinate anion, whether coordinated to the proton or to metal ions, can undergo self-association through mechanisms[22–24] associated with its aromatic character, which do not directly involve the formally recognised donor and acceptor groups (N, O and hydroxy H atoms). There is, of course, very substantial evidence in solid-state structures[1,5,17–21,28,43] of its capacity to promote oligomerisation through bridging coordination of the carboxylate groups, and facts such as the solvatochromism of the complex $[Fe(dipic)_2]^{2-}$[31] show that at least some other association mechanisms must remain effective in solution. A substantial remaining problem, recently recognised in general terms for both solid[23] and solution[44] systems, is to conduct a quantitative partitioning of the factors operative in any particular case of "supermolecule" formation. The present work provides at least circumstantial evidence that the energies of inter-dipicolinate interactions are sufficiently great to influence solid state reaction rates.

Experimental Section

General: Thermogravimetry: Weight loss and associated thermal changes resulting when ca. 20 mg samples of the complexes were heated between ca. 25 and 800 °C under air were monitored with a Rigaku "Thermoflex" instrument. Magnetometry: Measurements were made with a SQUID magnetometer (Quantum Design MPMS-7) at a magnetic field strength of 12 T in the temperature range 5–300 K. Samples were formed as small discs by compression of the powdered solids. Surface Area Determination: Surface areas for nitrogen adsorption were determined by the BET method on a Micrometer Gemini 2360 Surface Area Analyser, with a free space correction made using He.

Synthesis of the Precursor Complexes: Precipitation of $[Ln(dipic)_3]^{3-}$ anions from aqueous solution by the addition of cations such as $[Co(NH_3)_6]^{3+}$, $[Cr(en)_3]^{3+}$ and $[Cr(urea)_6]^{3+}$ is very efficient and we have previously described[1] the very simple syntheses of the resulting microcrystalline materials. In early attempts to prepare larger crystals of the various $[Co(NH_3)_6][Ln(dipic)_3]\cdot x\,H_2O$ solids

by digestion in the preparative supernatant solution and by recrystallisation from water, the Ln = La compound, in particular, was observed to be rather readily decomposed. In one apparently decomposed sample, however, orange crystals were found to be present and were then identified through crystallographic study as $[Co(NH_3)_6]$dipic·Cl·2 H_2O (**1**). In fact, this material is rather readily precipitated by simple addition of a molar equivalent of Na_2dipic to an aqueous solution of $[Co(NH_3)_6]Cl_3$, analysis of the bulk solid suggesting a slightly higher degree of hydration than deduced from the structure solution. (Found C 20.8, H 6.3, N 24.4; calculated for $C_7H_{21}ClCoN_7O_4$·2 H_2O: C 21.14, H 6.34, N 24.65; for $C_7H_{21}ClCoN_7O_4$·2.5 H_2O: C 20.67, H 6.44, N 24.11.)

Attempts, by numerous variations on liquid and vapour diffusion procedures, to obtain diffraction quality specimens of $[Co(NH_3)_6]$-$[Ln(dipic)_3]$·x H_2O for the full Ln series in an effort to systematically define phases present and their domains of existence yielded results that are erratic, the factors which determine the form of the solids remaining obscure. The principal method adopted for the growth of quite large crystals (sometimes 1 mm on edge) of all the $[Co(NH_3)_6][Ln(dipic)_3]$·$x$ H_2O compounds was to form a solution of the initial precipitate by slow addition of dilute HCl to its slurry with water until dissolution just occurred. (This was readily achieved with all the compounds up to Ln = Nd but with the heavier lanthanides it was apparent that an acid insoluble species, probably $[Ln(dipicH)(dipic)(OH_2)_2]$,[14] was formed, so that the initial solution, even when as dilute as 20 mg in 10 mL, was slightly cloudy. Fortunately, this did not seem to affect the quality of the crystals ultimately formed, though removal of this faint precipitate presumably decreased the recovery). After gravity filtration, this solution was then placed in a vapour diffusion cell with dilute aqueous ammonia in the outer compartment and the system allowed to stand under ambient conditions for extended periods. Several of the crystals used (particularly those involving the heavier rare earths, where there was a tendency for very long, thin needles to form) in the present structural studies were obtained only after more than a year of standing in contact with their supernatant solutions. Even then, for some elements no useful material was obtained at all.

Attempts to apply the above procedure for the growth of larger crystals of the $[Cr(urea)_6][Ln(dipic)_3]$ series were successful to the extent that materials obviously crystalline to the naked eye could be obtained but the crystals remained too small for single-crystal X-ray studies. Prolonged standing in the reaction mixture was to no advantage due to the hydrolysis of the $[Cr(urea)_6]^{3+}$ cation, which caused the initially deposited green crystals to redissolve and colourless crystalline solids to form under a violet supernatant solution. In the case of $[Cr(urea)_6][Eu(dipic)_3]$, a crystal drawn from the final product mass was characterised as [Eu(dipicH)(dipic)-$(OH_2)_2$]·4 H_2O, at the time of its isolation a new member of this Ln series, though its structure has since been determined.[14]

Powder Diffractometry: Measurements were made with a Siemens "Kristalloflex" D5000 diffractometer. For determination of the neodymium chromate structure, step-scan powder data were collected for 15°< 2θ < 100° (step size 0.02°, 8 s counting time per point) with Cu-K_α radiation, $\lambda = 1.5417_8$ Å, $T = 298(2)$ K. Rietveld refinement was carried out using the GSAS[35] suite of programs, with starting atomic models for the monazite (space group $P2_1/n$) and zircon (space roup $I4_1/amd$) forms of $NdCrO_4$ taken from the structures of monoclinic $PrPO_4$[37] and tetragonal $NdCrO_4$,[45] repectively. The profile (unit cells, zero-point error, 6-term background polynomial descriptors, pseudo-Voigt peak-shape parameters) and atomic parameters were progressively added to the model as variables in the usual fashion. The refinement converged to yield residuals, as defined in ref.[35] of $R_p = 8.75\%$, $R_{wp} = 11.94\%$, $R(F^2) = 5.78\%$ and $\chi^2 = 2.33$ (50 parameters, 424 reflections, 4248 profile points). The final observed, calculated and difference profiles are illustrated in Figure 6.

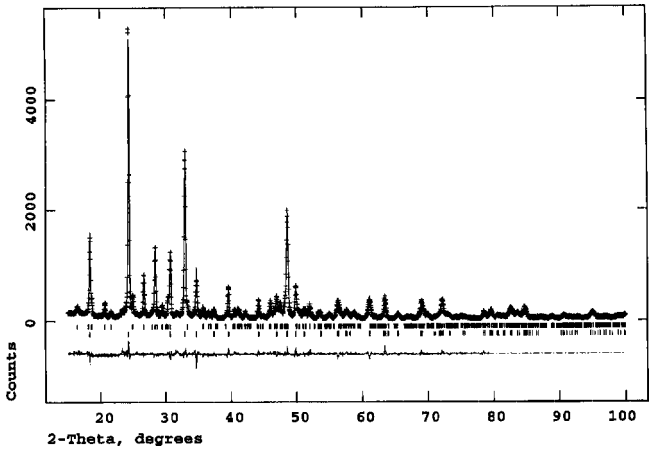

Figure 6. Observed, calculated (Rietveld) and difference intensity profiles for the powder X-ray diffraction pattern of $NdCrO_4$.

Room Temperature Single Crystal X-ray Structure Determinations: The structures of $[Co(NH_3)_6]$dipic·Cl·2 H_2O (**1**) and $[Co(NH_3)_6]$-$[Ce(dipic)_3]$·5 H_2O (**3a**) were determined first in Barcelona. Data sets (Enraf–Nonius CAD4 diffractometer; ω-scan mode; graphite-filtered Mo-K_α radiation, $\lambda = 0.7107_3$ Å) were measured at 293(2) K, with ψ-scan absorption corrections.

Structural studies of the $[Co(NH_3)_6][Ln(dipic)_3]$·$x$ H_2O series were extended in Western Australia (Ln = La(**2**), Ce(**3**), Pr(**4a**) (x = 5); Ln = Pr(**4b**), Sm(**5**), Tb(**6**), Er(**7**), Y(**8**) (x = 10); Ln = Tm(**9**), Lu(**10**) (x = 8.5). The frequent assumption that arrays of rare earth complexes can be adequately represented by studies of a single member or, alternatively, "early" and "late" members, has been effectively demolished as a reasonable presumption by studies of series such as the picrates[47–50] or chloride/terpyridyl[51] complexes (which is not to say that there are not series, such as the triflates,[52] which are represented by a single invariant, unambiguous structural type). The present array is no exception, offering suggestions of a series of subtlety comparable to that of the picrates, though more severe practical difficulties in respect of accessing appropriately crystalline specimens intrude here. As noted above, the gadolinium, terbium and lutetium specimens, for example, were grown by digestion at room temperature on a time scale of years (following slow precipitation over days by pH variation), and in most other cases several months' wait was involved. For several early samples, room temperature, single counter "four circle" diffractometer data sets were measured ($2\theta_{max}$ as specified; $2\theta/\theta$ scan mode; monochromatic Mo-K_α radiation, $\lambda = 0.7107_3$ Å; $T \approx$ 295 K), $N_{t(otal)}$ symmetry-equivalent reflections (where appropriate) being merged to N_r (unique) (R_{int} as quoted), N_o with $I > 3\sigma(I)$ being considered "observed" and used in the full-matrix, least-squares refinement on $|F|$ after Gaussian absorption correction. Conventional residuals R, R_w [statistical weights derivative of $\sigma^2(I) = \sigma^2(I_{diff}) + 0.0004\sigma^4(I_{diff})$] are quoted at convergence, neutral atom complex scattering factors being employed, computation using the Xtal 3.4 program system.[53] Significant nontrivial difference map residues were modelled as water molecule oxygen fragments, site occupancies being established by refinement; not infrequently, hydrogen atom dispositions could not be established with any cer-

tainty in association with fractionally occupied or "thermally smeared" fragments. For the extrema of the three major families, pertinent results are presented in the Figures and Tables, the latter showing the displacement envelopes for the non-hydrogen atoms at the 50% probability amplitude level, hydrogen atoms (where shown) having arbitrary radii of 0.1 Å.

A number of the determinations presented here were only finally accessible with the advent of an area-detector facility (Bruker AXS CCD instrument), spheres of data being measured at $T \approx 300$ K; preliminary data processing was carried out using proprietary software incorporating "empirical"/multiscan absorption correction, refinement using the Xtal 3.7 program system.[53]

Crystal/Refinement Data

1: $[Co(NH_3)_6]$dipic·Cl·2 H_2O, $C_7H_{25}ClCoN_7O_6$, M = 397.7, orthorhombic, space group $P2_12_12_1$ (D_2^4, No. 19), Z = 12, a = 7.123(1), b = 24.099(1), c = 28.670(2) Å, V = 4921 Å^3. $D_{calcd.}$ = 1.61$_1$ g cm^{-3}; μ_{Mo} = 12.5 cm^{-1}; specimen: 0.54 × 0.31 × 0.10 mm; $T_{min./max.}$ = 0.84. $2\theta_{max.}$ = 61°; N_t = 8408, N_r = 8623 (R_{int} = 0.107), N_o = 6408; R = 0.048, R_w = 0.121; n_v = 493, $|\Delta\rho_{max}|$ = 0.78 e Å^{-3}, $x_{abs.}$ = 0.24(2).

$[Co(NH_3)_6][Ln(dipic)_3]\cdot x\,H_2O$, $C_{21}H_{27}CoLnN_9O_{12}\cdot x\,H_2O$, triclinic, space group $P\bar{1}$ (C_i^1, No. 2), Z = 2.

(a) x = 5

2: Ln = La. M = 885.4. a = 10.454(5), b = 12.593(9), c = 13.438(7) Å, α = 102.69(5), β = 94.48(4), γ = 104.39(5)°, V = 1655 Å^3. $D_{calcd.}$ = 1.77$_6$ g cm^{-3}; μ_{Mo} = 18.6 cm^{-1}; specimen: 0.58 × 0.32 × 0.65 mm; $T_{min/max}$ = 0.63. $2\theta_{max}$ = 55°; N_t = 10703, N_r = 7591 (R_{int} = 0.025), N_o = 7064; R = 0.026, R_w = 0.037; n_v = 575, $|\Delta\rho_{max}|$ = 1.4 e Å^{-3}.

Variata: (x, y, z, U_{iso})$_H$ were refined throughout, except O(4,5) (water), for which they could not be definitively established. A further hemisphere of data was measured to $2\theta_{max}$ = 45°, hence R_{int} is quoted.

3: Ln = Ce. M = 886.6. a = 10.432(2), b = 12.583(2), c = 13.427(4) Å, α = 102.72(2), β = 94.32(2), γ = 104.27(2)°, V = 1651 Å^3. $D_{calcd.}$ = 1.78$_4$ g cm^{-3}; μ_{Mo} = 19.5 cm^{-1}; specimen: 0.24 × 0.19 × 0.14 mm; $T_{min/max}$ = 0.79 × $2\theta_{max}$ = 61°; N_t ($2\theta_{max}$ = 61°) = 10430, N_r = 9929, N_o = 4197; R = 0.071, R_w = 0.153; n_v = 448, $|\Delta\rho_{max}|$ = 1.4 e Å^{-3}.

Variata: Study of this complex (and of $[Co(NH_3)_6]$dipic·Cl·2 H_2O), undertaken in Barcelona, initiated the present series of determinations, the precision of which is improved for other Ln extending the domain of this phase. One attempt to improve crystal quality for the Ce species yielded better material but of a new, nonahydrate phase, described elsewhere.[15]

4a: Ln = Pr. M = 887.4. a = 10.4500(7), b = 12.5988(8), c = 13.4262(9) Å, α = 102.750(1), β = 94.180(1), γ = 104.305(1)°, V = 1655 Å^3. $D_{calcd.}$ = 1.78$_0$ g cm^{-3}; μ_{Mo} = 20.4 cm^{-1}; specimen: 0.30 × 0.20 × 0.12 mm; $T_{min/max}$ = 0.77. $2\theta_{max}$ = 58°; N_t (CCD data) = 22325, N_r = 8116 (R_{int} = 0.021), N_o [$F > 4\sigma(F)$] = 6830; R = 0.024, R_w = 0.030; n_v = 590, $|\Delta\rho_{max}|$ = 1.4 e Å^{-3}.

Variata: (x, y, z, U_{iso})$_H$ (all H) were refined. The unit cell dimensions of the Pr derivative are surprisingly similar to those of the La derivative, notwithstanding the clear and expected differences found in the Ln-N,O distances of the Ln coordination environments.

(b) x = 10

4b: Ln = Pr. M = 977.5. a = 16.416(1), b = 11.374(1), c = 11.0082(7) Å, α = 88.300(1), β = 72.577(1), γ = 70.863(1)°, V = 1847 Å^3. $D_{calcd.}$ = 1.75$_7$ g cm^{-3}; μ_{Mo} = 18.5 cm^{-1}; specimen: 0.29 × 0.20 × 0.18 mm; $T_{min/max}$ = 0.59 × $2\theta_{max}$ = 58°; N_t (CCD data) = 20623, N_r = 8994 (R_{int} = 0.068), N_o [$F > 4\sigma(F)$] = 7160; R = 0.078, R_w = 0.100; n_v = 481, $|\Delta\rho_{max}|$ = 5.9 e Å^{-3}.

Variata: Determinations of the members of this phase, although generally with larger specimen size, are inherently less precise than those of some other phases. Displacement parameters throughout the water molecules are generally high, some being modelled only with difficulty; associated hydrogen atoms were defined with reasonable certainty [though not for O(5,9)] but not refined, for the Ln = Er study, the present heavy and most precisely defined extremum.

5: Ln = Sm. M = 986.9. a = 16.302(6), b = 11.237(2), c = 10.978(2) Å, α = 88.26(1), β = 72.54(2), γ = 71.07(2)°, V = 1810 Å^3. $D_{calcd.}$ = 1.81$_1$ g cm^{-3}; μ_{Mo} = 21.6 cm^{-1}; specimen: 0.50 × 0.15 × 0.30 mm; $T_{min/max}$ = 0.83. $2\theta_{max}$ = 50°; N_t (sphere) = 12239, N_r = 6351 (R_{int} = 0.041), N_o [$I > 3\sigma(I)$] = 5735; R = 0.054, R_w = 0.074; n_v = 491, $|\Delta\rho_{max}|$ = 3.4 e Å^{-3}.

6: Ln = Tb. M = 995.5. a = 16.250(3), b = 11.227(1), c = 10.977(2) Å, α = 88.36(1), β = 72.48(2), γ = 71.23(1)°, V = 1803 Å^3. $D_{calcd.}$ = 1.83$_3$ g cm^{-3}; μ_{Mo} = 25.0 cm^{-1}; specimen: 0.55 × 0.18 × 0.45 mm; $T_{min/max}$ = 0.64. N_t (hemisphere to $2\theta_{max}$ = 50°, further hemisphere to 40°) = 11179, N_r = 8356 (R_{int} = 0.079), N_o [$I > 3\sigma(I)$] = 6851; R = 0.052, R_w = 0.068; n_v = 494, $|\Delta\rho_{max}|$ = 2.2 e Å^{-3}.

Variata: Hydrogen atoms were located in association with water molecule oxygen atoms O(1–3) only, for this adduct and for O(6–8) in addition for the Er adduct, for the Pr, Y and Sm adducts not at all.

7: Ln = Er. M = 1003.8. a = 16.216(2), b = 11.225(1), c = 10.982(1) Å, α = 88.377(2), β = 72.414(2), γ = 71.307(2)°, V = 1800 Å^3. $D_{calcd.}$ = 1.85$_2$ g cm^{-3}; μ_{Mo} = 28.8 cm^{-1}; specimen: 0.74 × 0.40 × 0.15 mm; $T_{min/max}$ = 0.54. $2\theta_{max}$ = 58°; N_t (CCD data) = 20903, N_r = 8768 (R_{int} = 0.035), N_o [$F > 4\sigma(F)$] = 7851; R = 0.039, R_w = 0.049; n_v = 491, $|\Delta\rho_{max}|$ = 3.0 e Å^{-3}.

8: Ln = Y. M = 925.5. a = 16.259(2), b = 11.275(1), c = 10.981(1) Å, α = 88.370(2), β = 72.389(2), γ = 71.239(2)°, V = 1811.$_5$ Å^3. $D_{calcd.}$ = 1.69$_7$ g cm^{-3}; μ_{Mo} = 21.5 cm^{-1}; specimen: 0.50 × 0.30 × 0.30 mm; $T_{min/max}$ = 0.66. $2\theta_{max}$ = 58°; N_t (CCD data) = 20168, N_r = 8886 (R_{int} = 0.036), N_o [$F > 4\sigma(F)$] = 5187; R = 0.060, R_w = 0.067; n_v = 491, $|\Delta\rho_{max}|$ = 2.1 e Å^{-3}.

(c) x = 8.5

9: Ln = Tm. M = 978.5. a = 16.250(6), b = 11.584(4), c = 10.449(4) Å, α = 110.905(9), β = 104.743(9), γ = 96.206(9)°, V = 1733 Å^3. $D_{calcd.}$ = 1.87$_5$ g cm^{-3}; μ_{Mo} = 31.2 cm^{-1}; specimen: 0.17 × 0.11 × 0.07 mm; $T_{min/max}$ = 0.79. $2\theta_{max}$ = 76°; N_t (CCD data) = 34830, N_r = 17907 (R_{int} = 0.033), N_o [$F > 4\sigma(F)$) = 12897; R = 0.041, R_w = 0.043; $|\Delta\rho_{max}|$ = 1.9 e Å^{-3}.

10: Ln = Lu. M = 984.5. a = 16.242(9), b = 11.591(5), c = 10.419(5) Å, α = 110.87(4), β = 104.96(5), γ = 96.05(4)°, V = 1728 Å^3. $D_{calcd.}$ = 1.91$_4$ g cm^{-3}; μ_{Mo} = 34.2 cm^{-1}; specimen: 0.18 × 0.30 × 0.35 mm; $T_{min/max}$ = 0.76. $2\theta_{max}$ = 50°; N_t (sphere) = 12081, N_r = 6091 (R_{int} = 0.069), N_o [$I > 3\sigma(I)$] = 4337; R = 0.048, R_w = 0.061; n_v = 480, $|\Delta\rho_{max}|$ = 2.9 e Å^{-3}.

Variata: The crystal decomposed isotropically by ca. 10% (as determined by periodic measures of standards), compensated by scaling. Water molecule hydrogen atoms were located in association with water molecule oxygen atoms O(1,5) only. O(9) has site occupancy 0.5; in the model for the Tm analogue, O(3–7) were modelled in terms of pairs of resolved fragments, with an additional fragment, "O(10)", hydrogen atoms only being located in association with O(1,2).

11: $[Eu(dipicH)(dipic)(OH_2)_2]_{(\infty|\infty)}\cdot 4H_2O = C_{14}H_{19}EuN_2O_{14}$, M = 591.3. Monoclinic, space group $P2_1/c$ (C_{2h}^5, No. 14), a = 14.002(1), b = 11.2293(9), c = 12.845(1) Å, β = 102.492(1)°, V = 1972 Å^3. $D_{calcd.}$ (Z = 4) = 1.99$_1$ g cm^{-3}; μ_{Mo} = 32.6 cm^{-1}; specimen: 0.15 × 0.15 × 0.15 mm; $T_{min/max}$ = 0.84. $2\theta_{max}$ = 50°; N_t (CCD data) = 21787, N_r = 4999 (R_{int} = 0.025), N_o [$F > 4\sigma(F)$] = 4290; R = 0.025, R_w = 0.019; $|\Delta\rho_{max}|$ = 1.15(6) e Å^{-3}.

Variata: (x, y, z, U_{iso})$_H$ (all H) were refined. At the time of this determination, cell and coordinate settings were based upon those of the known La analogue.[14a,14b] In the present, Eu–N are 2.566(2), 2.564(2) Å, Eu−O(dipic) 2.433(2)–2.512(2) and Eu−O(water) 2.390(2)–2.440(2) Å.

CCDC-252240 to -252251 contain the supplementary crystallographic data for this paper. These data can be obtained free of charge from The Cambridge Crystallographic Data Centre via www.ccdc.cam.ac.uk/data_request/cif.

Acknowledgments

We thank Dr Jordi Rius (Barcelona) for calculation of the powder X-ray diffraction pattern expected for $[Co(NH_3)_6][Ce(dipic)_3]\cdot 5H_2O$, and the Australian Research Council for partial support of this work.

[1] a) P. A. Brayshaw, J-C. G. Bünzli, P. Froidevaux, J. M. Harrowfield, Y. Kim, A. N. Sobolev, *Inorg. Chem.* **1995**, *34*, 2068–2076; b) J. M. Harrowfield, Y. Kim, B. W. Skelton, A. H. White, *Aust. J. Chem.* **1995**, *48*, 807–823; c) P. A. Brayshaw, J. M. Harrowfield, A. N. Sobolev, *Acta Crystallogr. Sect. C* **1995**, *51*, 1799–1802.

[2] E. Hukowska, J. P. Riehl, *Inorg. Chem.* **1995**, *34*, 5615–5621 and references cited therein.

[3] J. Dexpert-Ghys, C. Picard, A. Taurines, *J. Incl. Phenom. Macrocyclic Chem.* **2001**, *39*, 261–267.

[4] N. Ouali, B. Bocquet, S. Rigault, P-Y. Morgantini, J. Weber, C. Piguet, *Inorg. Chem.* **2002**, *41*, 1436–1445; see also references given in ref.[1a]

[5] Structural studies of various hydrated salts of the tris(dipicolinato)lanthanide(III) anions not acknowledged in our earlier publications include a) S. Hu, Z. Dong, H. Zhang, Q. Liu, *J. Xi'an Med. Univ.* **1989**, *28*, 279–283, 514–518; b) T. Gin, J. Liu, H. Zhang, C. Huang, G. Xu, Y. Han, N. Shi, *J. Chin. Rare Earth Soc.* **1991**, *9*, 97–100. Recent spectroscopic work has included corroboration of early structural data (see references [17–20] on $Na_3[Ln(dipic)_3]\cdot 13H_2O$ species; c) C. Reinhard, H. U. Güdel, *Inorg. Chem.* **2002**, *41*, 1048–1055. Some related $Ln_2(dipic)_3$ species have been recently characterised by structural studies, see d) S. K. Ghosh, P. K. Bharadwaj, *Inorg. Chem.* **2004**, *43*, 2293–2298.

[6] A. Roy, K. Nag, *J. Inorg. Nucl. Chem.* **1978**, *40*, 1501–1505.

[7] P. S. Devi, M. S. Rao, *Mater. Lett.* **1993**, *16*, 14–21.

[8] M. Insausti, M. K. Urtiaga, R. Cortés, J. L. Mesa, M. I. Arriortua, T. Rojo, *J. Mater. Chem.* **1994**, *4*, 1867–1870.

[9] Y. Sadaoka, E. Traversa, M. Sakamoto, *Chem. Lett.* **1996**, 177–178.

[10] P. S. Devi, M. S. Rao, *J. Therm. Anal.* **1997**, *48*, 909–916.

[11] A. Gonzalez, E. Martinez Tamayo, A. Beltran Porter, V. Cortes Corberan, *Catal. Today* **1997**, *33*, 361.

[12] See, for example: L. G. Tejuca, J. L. G. Fierro, J. M. D. Tascon, *Adv. Catal.* **1989**, *36*, 237–328; D. J. M. Bevan, E. Summerville (chapter 28), C. P. Khattak, F. F. Y. Wang (chapter 29), in: *Handbook on the Chemistry and Physics of the Rare Earths* (Eds.: K. A. Geschneidner, Jr., L. Eyring), vol. 3, North-Holland, Amsterdam, **1978**.

[13] M. Chen, H-Q. Huang, X-M. Zheng, M. A. Morris, *Aust. J. Chem.* **2002**, *55*, 757–760.

[14] a) (Ln = La) P. Gurriero, U. Castellato, S. Sitran, P. A. Vigato, R. Graziani, *Inorg. Chim. Acta* **1987**, *133*, 337–345; b) (Ln = Nd) J-L. Wang, T-Z. Jin, J-K. Liu, H-Z. Zhang, C-H. Huang, *Chinese J. Inorg. Chem. (Wuji Huaxe Xuebao)* **1992**, *8*, 180–183; c) (Ln = Eu, Gd, Tb, Dy, Ho, Er, Yb) A. Fernandes, J. Dexpert-Ghys, C. Brouca-Cabarrecq, *Polyhedron* **2001**, *20*, 2385–2391; d) (Ln = Ce, Pr) S. K. Ghosh, P. K. Bharadwaj, *Inorg. Chem.* **2003**, *42*, 8250–8254.

[15] J. M. Harrowfield, B. W. Skelton, A. H. White, submitted to *Cryst. Growth Des.* **2004**.

[16] D. A. House, in: *Comprehensive Coordination Chemistry* (Eds.: J. A. McCleverty, R. D. Gillard, G. Wilkinson), Pergamon Press, Oxford, **1987**, vol. 2, Ch. 13.1, p. 21, provides a summary of structural data relating to various $[Co(NH_3)_6]^{3+}$ salts.

[17] J. Albertsson, *Acta Chem. Scand.* **1970**, *24*, 1213–1229.

[18] J. Albertsson, *Acta Chem. Scand.* **1972**, *26*, 1023–1044.

[19] J. Albertsson, *Acta Chem. Scand.* **1972**, *26*, 1005–1017.

[20] J. Albertsson, *Acta Chem. Scand.* **1972**, *26*, 985–1004.

[21] G. Swarnabala, M. V. Rajasekharan, *Inorg. Chem.* **1998**, *37*, 1483–1485.

[22] A. K. Hall, J. M. Harrowfield, B. W. Skelton, A. H. White, *Acta Crystallogr., Sect. C* **2000**, *56*, 407–411.

[23] Comprehensive analyses of both "offset face-to-face" (conventional π- stacking) and "edge-to-face" interactions between aromatic groups in metal complexes have been given by a) W. B. Jennings, B. M. Farrell, J. F. Malone, *Acc. Chem. Res.* **2001**, *34*, 885–895; b) V. Russell, M. L. Scudder, I. G. Dance, *J. Chem. Soc. Dalton Trans.* **2001**, 789–799; b) I. G. Dance, M. L. Scudder, *J. Chem. Soc. Chem. Commun.* **1995**, 1039–1040; *Chem. Eur. J.* **1996**, *2*, 481–486; *J. Chem. Soc. Dalton Trans.* **1996**, 2755–2769; **1998**, 1341–1350, 3155–3166, 3167–3176; c) C. Janiak, *J. Chem. Soc. Dalton Trans.* **2000**, 3885; d) Z-H. Liu, C-Y. Duan, J-H. Li, Y-J. Liu, Y-H. Mei, X-Z. You, *New J. Chem.* **2000**, *24*, 1057–1062.

[24] a) See:J. M. Harrowfield, *J. Chem. Soc. Dalton Trans.* **1996**, 3165–3171 and references cited therein; b) L. Troxler, J. M. Harrowfield, G. Wipff, *J. Phys. Chem. A* **1998**, *102*, 6821–6830; c) J. M. Harrowfield, R. P. Sharma, T. M. Shand, B. W. Skelton, A. H. White, *Aust. J. Chem.* **1998**, *51*, 707–722; d) J. M. Harrowfield, R. P. Sharma, B. W. Skelton, A. H. White, *Aust. J. Chem.* **1998**, *51*, 723–734; e) J. M. Harrowfield, R. P. Sharma, B. W. Skelton, A. H. White, *Aust. J. Chem.* **1998**, *51*, 735–745; f) J. M. Harrowfield, R. P. Sharma, B. W. Skelton, A. H. White, *Aust. J. Chem.* **1998**, *51*, 747–760; g) J. M. Harrowfield, R. P. Sharma, B. W. Skelton, A. H. White, *Aust. J. Chem.* **1998**, *51*, 761–774; h) J. M. Harrowfield, R. P. Sharma, B. W. Skelton, P. Vengulopalam, A. H. White, *Aust. J. Chem.* **1998**, *51*, 775–784; i) J. M. Harrowfield, R. P. Sharma, B. W. Skelton, A. H. White, *Aust. J. Chem.* **1998**, *51*, 785–793.

[25] a) S. Burnet, A. K. Hall, J. M. Harrowfield, G. A. Koutsantonis, V. Sanford, D. Sauter, B. W. Skelton, A. H. White, *Supramol. Chem.* **2003**, *15*, 291–312; b) A. A. Soudi, J. M. Harrowfield, G. H. Shahverdizadeh, *Supramol. Chem.* **2003**, *15*, 367–373.

[26] J. M. Harrowfield, G. A. Koutsantonis, B. W. Skelton, A. J. Strong, A. H. White, submitted to *Cryst. Growth Des.* **2004**.

[27] J. M. Harrowfield, G. A. Koutsantonis, G. L. Nealon, B. W. Skelton, A. H. White, submitted to *Inorg. Chem.* **2004**.

[28] J-C. G. Bünzli, P. Froidevaux, J. M. Harrowfield, *Inorg. Chem.* **1993**, *32,* 3306–3311.

[29] See, for example: R. J. Geue, M. R. Snow, *Inorg. Chem.* **1977**, *16*, 231–241; H. Okazaki, U. Sakaguchi, H. Yoneda, *Inorg. Chem.* **1983**, *22*, 1539–1542 and references cited therein.

[30] M. W. Hosseini, R. Ruppert, P. Schaeffer, A. De Cian, N. Kyritsakas, J. Fischer, *J. Chem. Soc. Chem. Commun.* **1994**, 2135–2136.

[31] P. Lainé, A. Gourdon, J-P. Launay, *Inorg. Chem.* **1995**, *34*, 5129–5137.

[32] D. B. Wiles, R. A. Young, *J. Appl. Crystallogr.* **1981**, *14*, 149–151.

[33] R. J. Hill, C. J. Howard, *AAEC Report* **1986**, *M112*.
[34] I. C. Madsen, R. J. Hill, *Powder Diffraction* **1990**, *5*, 195–199.
[35] A. C. Larson, R. V. von Dreele, *GSAS User Guide*, Los Alamos National Laboratory, New Mexico, USA, **1995**.
[36] A. S. Wexler, J. H. Seinfeld, *Atmospheric Environment* **1991**, *25A*, 2731–2748.
[37] Y. Ni, J. M. Hughes, A. N. Mariano, *Amer. Miner.* **1995**, *80*, 21–26.
[38] K. J. Range, H. Meister, U. Klement, *Zeit. Naturforsch.* **1990**, *B45*, 598–602.
[39] JCPDS Card 16–880.
[40] R.D Shannon, *Acta Crystallogr. Sect. A* **1976**, *32*, 751–767.
[41] M. Taylor, R. C. Ewing, *Acta Crystallogr. Sect. B* **1978**, *34*, 1074–1079.
[42] A. Morales-Sanchez, F. Fernandez, *J. Alloys and Compounds* **1963**, *201*, 161–165; H. Walter, H. G. Kahle, K. Mulder, H. C. Schopper, H. Schwarz, *Int. J. Magnetism* **1973**, *5*, 129–135;E. F. Bertraut, G. Bassi, G. Buisson, P.Burlet, J. Chappert, A. Delapalme, J. Mareschal, G. R. Rault, R. Aleonard, R. Pauthenet, J. B. Rebouillat, *J. Appl. Phys.* **1966**, *37*, 1038–1039.
[43] P. Lainé, A. Gourdon, J-P. Launay, *Inorg. Chem.* **1995**, *34*, 5138–5149, 5150–5155, 5156–5165.
[44] R. B. Martin, *Chem. Rev.* **1996**, *96*, 3043–3064.
[45] G. Buisson, F. Bertaut, J. Mareschal, *C. R. Acad. Sci. Paris* 19**64**, *259*, 411–415.
[46] A. J. C. Wilson (Ed.), *International Tables for Crystallography*, vol. C, Kluwer Academic Publishers, Dordrecht, **1992**.
[47] J. M. Harrowfield, Lu Weimin, B. W. Skelton, A. H. White, *Aust. J. Chem.* **1994**, *47*, 321–337.
[48] J. M. Harrowfield, Lu Weimin, B. W. Skelton, A. H. White, *Aust. J. Chem.* **1994**, *47*, 339–348.
[49] J. M. Harrowfield, Lu Weimin, B. W. Skelton, A. H. White, *Aust. J. Chem.* **1994**, *47*, 349–358.
[50] J. M. Harrowfield, Lu Weimin, B. W. Skelton, A. H. White, *Aust. J. Chem.* **1994**, *47*, 359–364.
[51] C. J. Kepert, Lu Weimin, B. W. Skelton, A. H. White, *Aust. J. Chem.* **1994**, *47*, 365–384.
[52] J. M. Harrowfield, D. L. Kepert, J. M. Patrick, A. H. White, *Aust. J. Chem.* **1983**, *36*, 483–492.
[53] a) S. R. Hall, G. S. D. King, J. M. Stewart (Eds.), *The Xtal 3.4 User's Manual* (University of Western Australia: **1995**); b) S. R. Hall, D. J. Du Boulay, R. Olthof-Hazekamp (Eds.) *The Xtal 3.7 System*, University of Western Australia, **2000**.

Received: October 14, 2004

